Structure, Vol. 10, 901–911, July, 2002, ©2002 Elsevier Science Ltd. All rights reserved. PII S0969-2126(02)00781-5

SH3-SH2 Domain Orientation in Src Kinases: NMR Studies of Fyn

Tobias S. Ulmer,[1] Jörn M. Werner,[1] and Iain D. Campbell[1,2,3]
[1]Department of Biochemistry
University of Oxford
South Parks Road
Oxford OX1 3QU
United Kingdom
[2]Oxford Centre for Molecular Sciences
University of Oxford
South Parks Road
Oxford OX1 3QT
United Kingdom

Summary

The regulatory domains of Src family kinases SH3 and SH2 suppress Src activity when bound to the catalytic domain. Here, the isolated SH3-SH2 fragment from the Src family member Fyn (FynSH32) is studied by NMR. The properties of this fragment are expected to be similar to the domains in the active state, where they are dissociated from the catalytic domain. Cross-communication between SH3 and SH2 of FynSH32, measured by chemical shift perturbation, was found to be small. Diffusion and alignment anisotropy measurements showed that SH3 and SH2 of peptide-bound FynSH32 are significantly coupled but still exhibit some interdomain flexibility. The observed average domain orientation indicates that a large SH3-SH2 domain closure is required to reach the inactive state. The implications of these results for Src regulation are discussed.

Introduction

Fyn is a member of the Src nonreceptor tyrosine kinase family, which comprises highly conserved signaling proteins involved in a wide range of cellular functions. Src family kinases are comprised of a catalytic tyrosine kinase domain preceded by two ligand binding regulatory domains, SH3 and SH2. Regulation of kinase activity is mediated by the formation of an intramolecular complex between SH3 and/or SH2 and the kinase domain. Phosphorylated Tyr527 in the C-terminal kinase domain tail and part of the SH2-kinase domain linker provide intramolecular ligands for SH2 and SH3, respectively, leading to an assembled inactive kinase state (Figure 1) [1–3]. Dephosphorylation of Tyr527 or the binding of external ligands to the SH3 and/or SH2 domain results in dissociation of SH3 and/or SH2 from the kinase domain and self-activation of Src kinases (reviewed in [4, 5]). For full catalytic activity, dissociation of both SH3 and SH2 from the kinase domain is required [6, 7]. The extent of coupling between SH3 and SH2 appears to play a significant role in this activation process, since substitution of SH3-SH2 linker residues with glycines activates c-Src [8]. Molecular dynamics simulations of c-Src and Hck kinase suggested a dynamic, Src assembly state-dependent SH3-SH2 coupling that is tight in the assembled inactive state and becomes more flexible when the phosphorylated kinase domain tail (Y527) no longer binds to the SH2 domain [8]. The existence of a "snap lock" mechanism for the SH3-SH2 domain-domain interface has been proposed [8].

The present NMR study examines the isolated SH3-SH2 fragment from the Src family kinase Fyn (FynSH32) in solution. Fyn is highly homologous to most other Src family kinases, e.g., it shares overall sequence homologies of 74.4% and 63.1% with c-Src and Hck, respectively; therefore, the results obtained are expected to be generally applicable to Src family kinases. Isolated SH3-SH2 fragments are expected to correspond to the active, dissociated SH3-SH2 state, where the two domains are uncoupled from the kinase domain. The structures of assembled inactive Src states are known (e.g., Figure 1) and crystal structures of isolated SH3-SH2 fragments are available; nevertheless, it is of considerable interest to have more information about the relative SH3-SH2 domain orientation and interdomain coupling of SH3-SH2 fragments in solution. Therefore, the extent of Fyn SH3-SH2 crosscommunication and interdomain coupling is characterized here. The average Fyn SH3-SH2 domain orientation is determined and compared to the SH3-SH2 orientation in the inactive, kinase-bound state to provide insight into Src kinase regulation. Cross-communication between SH3 and SH2 of FynSH32, measured by chemical shift perturbation, was found to be small. Diffusion and alignment anisotropy measurements showed that SH3 and SH2 of peptide-bound FynSH32 are significantly coupled but still exhibit some interdomain flexibility. A large SH3-SH2 domain closure is required for peptide-bound FynSH32 to reach the inactive, kinase-bound SH3-SH2 orientation.

Results and Discussion

Crosscommunication between SH3 and SH2 of FynSH32

The chemical shift of a nucleus is very sensitive to its local structural environment. Here, backbone $^{1}H^{N}$ and ^{15}N chemical shift changes between peptide-bound and free FynSH32 states were used to explore the propagation of structural changes (crosscommunication) from the ligand binding site on one domain to the adjacent domain.

Three different peptide ligands were employed: a proline-rich peptide, derived from focal adhesion kinase FAK3A, which binds to SH3 of FynSH32 with a K_D of $\sim 3.2 \times 10^{-5}$ M [9, 10]; HMTA, a phosphopeptide derived from the hamster polyomavirus middle T antigen [11], which binds to the Src SH2 domain with a K_D of $2 \times$

[3]Correspondence: idc@bioch.ox.ac.uk

Key words: domain orientation; dynamic domain coupling; residual dipolar coupling; rotational diffusion anisotropy; Src kinase; SH3-SH2

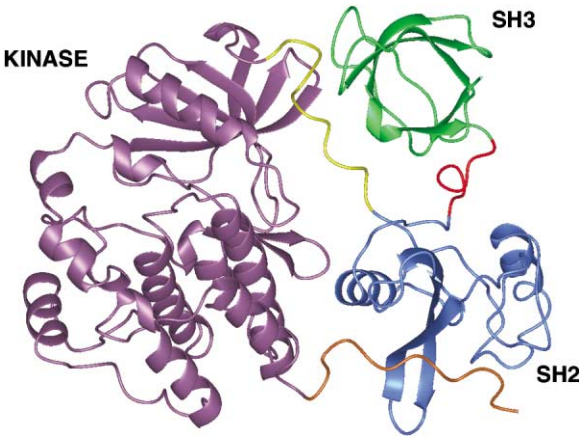

Figure 1. Cartoon Representation of Human c-Src Kinase in the Assembled, Inactive State

In the assembled inactive Src state, SH3 binds to the SH2-kinase domain connector (yellow), and SH2 binds to the phosphorylated kinase domain tail (Y527; orange). The SH3-SH2 linker is shown in red.

10^{-7} M [12], and SM1, a phosphopeptide derived from residues 522–532 of the regulatory tail of human Src, which binds with a K_D of 2.9×10^{-5} M [12]. The different affinities of SM1 and HMTA can be explained, simplistically [12], by their SH2 binding sequences, pYQPG and pYEEI, which resemble a one- and two-pronged plug, respectively, inserting into a two-holed socket (the SH2 domain) [13].

Figure 2A shows the chemical shift changes communicated from SH2 to SH3 upon peptide binding to SH2. The direct ligand-induced shift changes occurring in SH2 are not shown, since the binding of peptide ligands to individual Fyn SH3 and SH2 domains has been studied previously in great detail [14–16]. Differences in the shifts induced by SM1 and HMTA (Figure 2A) show that the extent of shift changes is related to the affinity of the peptide and the mode of binding (see e.g., the $^1H^N$ shift of L86). $^1H^N$ shift changes of >0.01 ppm or ^{15}N shift changes of >0.1 ppm were considered significant, thus identifying the resonances of residues L86, T97, H104, A139, and D142 as being perturbed. The extent of chemical shift changes in SH3 upon peptide binding to SH2 is similar to that found for SrcSH32 [17]. Figure 2B shows the shift changes communicated from SH3 to SH2 upon peptide binding to the SH3 domain. Here, for practical reasons (less signal overlap and reduced $^1H^N$ solvent chemical exchange) SH32*FAK3A*HMTA was compared to SH32*HMTA. For SH2, the resonances of residues I144, W149, G152, Q225, and S246 could be identified as significantly shifted. For completeness, we note that similar results were obtained for the comparison of SH32*FAK3A*HMTA with SH32*FAK3A and for the comparison of SH32*FAK3A with SH32 (data not shown).

Figure 3 indicates the location of all residues with an observed shift difference above the chosen cutoff values, except T97 and H104, on the crystal structure of free FynSH32. The effects observed for T97 and H104 may not be due directly to ligand binding to the SH2 domain, since T97 is within the ligand binding site of the SH3 domain (Figure 3B). HMTA contains a $P(x)_5P$ sequence motif, which is somewhat similar to the SH3 consensus binding sequences [18], so the observed shift is probably due to weak binding of excess HMTA peptide. H104, which is also far from the linker region, is suspected to be very sensitive to small changes in pH near its pK_a value. All other identified residues are either within the linker (D142 and I144) or close to the linker (L86, A139, W149, G152, Q225, and S246), indicative of changes in domain-linker contacts. Upon close inspection of the domain-linker region, it appears that L86 and G152, the only residues not in direct contact with linker residues (Figure 3), are coupled to the linker via V141 and Y150, respectively. The $^1H^N$ nucleus of L86 packs against the side chain of V141 (Figure 3A), and its shift is likely to reflect small structural changes of the side chain of V141, whose own $^1H^N$-^{15}N nuclei are actually further away from its side chain and do not exhibit shift changes (Figure 2A). Similarly, the $^1H^N$ nucleus of G152 directly faces the aromatic ring of Y150 (Figure 3B). Furthermore, the detected shift changes on the SH2 domain (Figure 3A) suggest that linker residues, which have been unobservable here (Figure 2), are involved in domain-linker contacts.

The small magnitude of the chemical shift changes propagated into the respective adjacent domain indicates that the underlying structural changes are also small. These results suggest that the occupancy of one binding site has no influence on the occupancy of the binding site on the adjacent domain, and binding site occupancy does not significantly affect interdomain coupling between SH3 and SH2 of FynSH32.

Interdomain Coupling between SH3 and SH2 of Peptide-Bound FynSH32

In this section the magnitude of the alignment and, particularly, the diffusion tensors of SH3 and SH2 domains of peptide-bound FynSH32 (FynSH32*FAK3A*HMTA) are compared, to obtain information about the extent of motional coupling between SH3 and SH2 (interdomain coupling). Peptide-bound FynSH32 is expected to correspond to SH3-SH2 in the active, dissociated Src state (when bound to external ligands); therefore, insight into the dynamics of this state was sought. The results are interpreted within the two limiting cases of a fully flexible and a fully rigid domain linkage. In the fully flexible case, the diffusion tensor parameters would correspond to parameters observed for individual isolated SH3 and SH2 domains. In the fully rigid case, the diffusion tensor parameters would describe one globular structure, with experimental parameters similar to the parameters calculated from the (rigid) FynSH32 crystal structure.

Backbone ^{15}N longitudinal and transverse relaxation times, T_1 and T_2, are sensitive to rotational diffusive motions and were used to determine the molecular diffusion tensors [19, 20]. In certain liquid crystalline media, such as bicelles, a small degree of molecular alignment with the magnetic field is induced on cosolute molecules [21]. This alignment results in residual dipolar couplings (RDCs) between H-N nuclei, which depend on the nature of the alignment. In bicelle medium, the alignment is molecular shape dependent, hence, also dependent on diffusive motions. Experimentally, the diffusion and

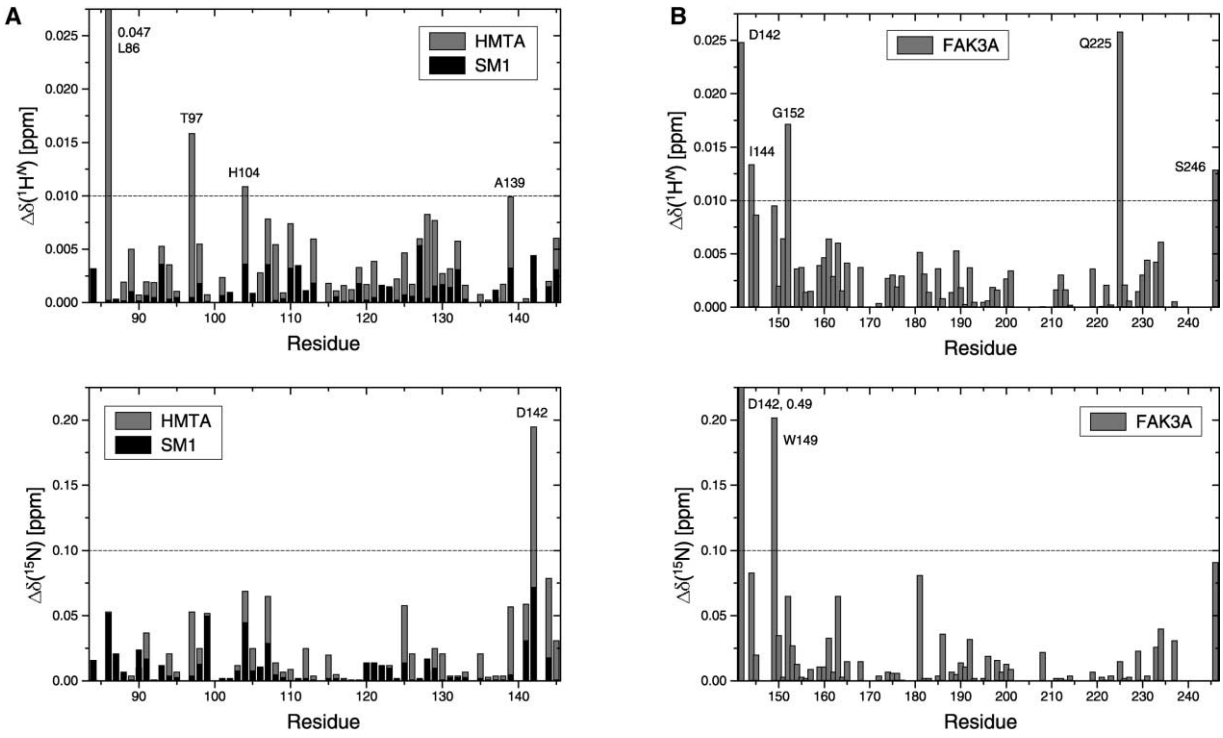

Figure 2. Absolute ^{1}H and ^{15}N Chemical Shift Differences between Free FynSH32 and FynSH32 Bound to Peptide Ligands

(A) Chemical shifts for residues 84–145 (the SH3 domain plus linker) of FynSH32 are compared with residues 84–145 of FynSH32*SM1 (black columns) and of FynSH32*HMTA (gray columns).

(B) Chemical shifts for residues 142–246 (the linker plus SH2 domain) of FynSH32*HMTA are compared with residues 142–246 of FynSH32*HMTA*FAK3A.

Chemical shift changes of the domains to which the peptides bind directly are not shown. Linker residues S143 and A146–E148 could not be observed, probably due to rapid ^{1}H solvent chemical exchange at pH 7.0. The other gaps are due to signal overlap or rapid solvent exchange of the corresponding ^{1}H nuclei.

alignment tensors can be determined in an analogous fashion. An error function, χ^2, describing the agreement between experimental and calculated T_1/T_2 ratios and RDCs, respectively, is minimized to find the tensor parameters that best reproduce the experimental results. H-N internuclear coordinates are generally required in this process and render the quality of the fits, i.e., the value of χ^2, dependent on the accuracy of the input H-N coordinates. Consequently, χ^2 can also be used to judge the accuracy of the input structure. For free FynSH32 a

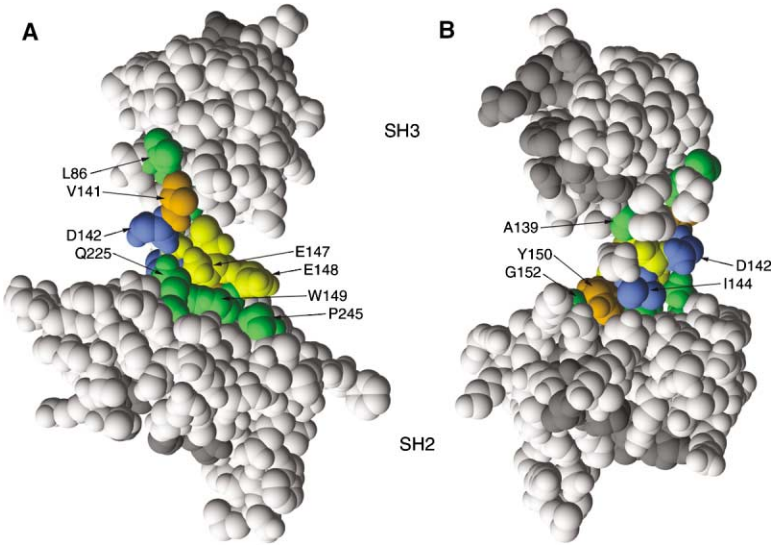

Figure 3. Chemical Shift Changes Propagated between SH3 and SH2 of FynSH32 upon Peptide Binding Mapped on the Crystal Structure of FynSH32 (B Form)

Linker residues affected by peptide binding (D142 and I144) are shown in blue. Linker residues S143 and A146–E148, which could not be observed, are shown in yellow. Residues affected by peptide binding to the adjacent domain (L86, A139, W149, G152, Q225, and S246), revealing domain-linker contacts, are shown in green (S246 was not observable in the crystal structure; therefore, P245 was colored). In (A), V141, whose side chain packs against $^{1}H^{N}$ of L86, is shown in orange. In (B), Y150, whose aromatic ring faces $^{1}H^{N}$ of G152, is shown in orange. All other residues are shown in gray. The ligand binding regions of FynSH32 are highlighted in dark gray.

2.6 Å X-ray crystal structure [10], with two molecules per asymmetric unit cell, provides two independent coordinate sets, termed A and B, for the fits. Crystal structures of other SH3 and SH2 domains, free and peptide bound, show that the backbone conformation is virtually unchanged upon peptide binding [13, 22, 23], so the assumption was made here that this structure can also provide input coordinates for peptide-bound FynSH32. Four different diffusion tensors of increasing complexity were tested: an isotropic tensor that is independent of any molecule coordinates, an axially symmetric tensor that can be either prolate or oblate, and a fully asymmetric tensor. F test statistics were used to assess whether a more complex tensor gives a statistically significant improvement in the description of the experimental data.

Table 1 shows the diffusion tensor parameters, experimental χ^2, and the 90% confidence limit, $\chi^2_{(\alpha = 0.10)}$, derived from Monte Carlo simulations as well as F test-derived Q values [24] for the four diffusion models of SH3 and SH2, respectively, of peptide-bound FynSH32 calculated with the FynSH32 A and B coordinates. For the SH3 domain, experimental χ^2 values lie outside the $\chi^2_{(\alpha = 0.10)}$ for all but the fully asymmetric diffusion tensor of the B form of SH3 (B SH3), indicating that this is the only acceptable model. Examination of the input T_1/T_2 ratios shows that the sampling of H-N vector orientations for SH3 is good, despite a relatively small dataset (Figure 4A). Therefore, the significantly lower χ^2 values obtained for the B form of SH3 compared to those obtained for A SH3 suggest that the B coordinates agree better with the solution structure of (peptide-bound) FynSH32 than do the A coordinates. The Q values (for B SH3) also show that the use of the fully asymmetric tensor over the other, simpler tensors is statistically justified (Table 1). Thus, SH3 of peptide-bound FynSH32 tumbles with a fully asymmetric diffusion tensor, with anisotropy, $2D_{zz}/(D_{xx}+D_{yy})$, of 1.48 ± 0.08 and D_{xx}/D_{yy} ratio of 0.62 ± 0.04 (Table 1; B SH3 values). Similar examination of the data for the SH2 domain of peptide-bound FynSH32 indicates that fits using an axially symmetric, prolate, and fully asymmetric tensor are of acceptable quality for both A and B coordinates (Table 1). The sampling of H-N vector orientations is also good (Figure 4B), and there are less-pronounced differences between the experimental χ^2 values for the SH2 A and B coordinates. The Q values for SH2 show that the adoption of the fully anisotropic tensor is statistically not justified in this case (Table 1). Thus, the SH2 domain of peptide-bound FynSH32 tumbles with an axially symmetric, prolate tensor with diffusion anisotropy of 1.59 ± 0.07 (Table 1; A SH2 value).

Table 2 shows the obtained alignment tensors for SH3 and SH2 of ligand-bound FynSH32 from order matrix analysis [25] of residual dipolar couplings (RDCs) measured in bicelle solution. The range of RDCs, as reflected by the values of A_a, is similar for SH3 and SH2 and slightly larger for SH2, an indication for their partial coupling and a slightly stronger alignment of SH2, in accordance with its more asymmetric shape (higher diffusion anisotropy). In the present case, the low alignment tensor rhombicity, η, of ≤0.09 for SH2 reflects the axially symmetric rotational diffusion of SH2, while the higher η of 0.21 for SH3 (B form) reflects the fully asymmetric rotational diffusion of SH3. Thus, the characteristics of the SH3 and SH2 diffusion tensors are found again in their respective alignment tensors in bicelle medium. In further agreement with the diffusion tensor analysis, lower χ^2 values are again obtained for the B SH3 coordinates compared to the A SH3 ones, while the χ^2s for SH2 are again comparable for the A and B coordinates (Table 2). The good correlation coefficients between experimental and back-calculated RDCs of 0.983 for B SH3 and 0.979 for B SH2 also show that the usage of the free FynSH32 backbone coordinates to describe the backbone coordinates of the peptide-bound state is adequate (for the selected subset of residues).

A lower limit for the diffusion anisotropy, for the fully flexible coupled SH3-SH2 case, is estimated from the diffusion anisotropies determined for the isolated SH3 and SH2 domains of Abelson kinase, with values of 1.10 ± 0.05 and 1.12 ± 0.06, respectively [26]. An upper limit for the diffusion anisotropy, for the fully rigid coupled SH3-SH2 case, is estimated from the FynSH32 crystal structure (Figures 3 and 5A) using a bead model [27, 28], with values of 1.61 for A, and 1.67 for B, FynSH32. When these limiting values are compared to the measured diffusion anisotropies of 1.48 ± 0.08 for SH3 and 1.59 ± 0.07 for SH2, it is apparent that SH3 and SH2 of peptide-bound FynSH32 are considerably coupled but still exhibit some interdomain flexibility (i.e., the domains are in an "intermediately" coupled state). The interdomain flexibility is also reflected by the differences in isotropic correlation times (0.66 ± 0.09 ns), diffusion anisotropy (0.11 ± 0.10), and molecular alignment in bicelles (Table 2) between SH3 and SH2. In light of the finding that substitution of SH3-SH2 linker residues with glycine residues activates the close Fyn homolog c-Src kinase [8], the extent of SH3-SH2 coupling seems to be "tuned" in evolution to be tight enough to allow the formation of a stable assembled inactive Src complex yet also flexible enough to allow the SH3 and SH2 domains to bind to alternative, external ligands in the dissociated, active Src state.

Finally, we briefly comment on the effects of peptide binding on the interdomain coupling of FynSH32 and compare it with other isolated SH3-SH2 fragments. Free FynSH32 was found to be partially aggregated (see Experimental Procedures) and, hence, unfortunately, not amenable to a full analysis, as presented for peptide-bound FynSH32. The isotropic correlation times of SH3 and SH2 of free FynSH32, which, crudely, measure the rate of rotational tumbling, differ by 0.9 ± 0.2 ns, as we have reported previously [10]. Although aggregation will affect this value, judging from the similar difference observed for peptide-bound FynSH32 (0.66 ± 0.09 ns), the interdomain coupling appears not to be substantially affected by peptide binding to SH3 and SH2. This observation is in agreement with the small chemical shift changes in the domain-linker region (Figures 2 and 3).

For the isolated SH3-SH2 fragment of the Src family kinase Hck (HckSH32), which is structurally highly homologous to FynSH32 [10], deuterium exchange studies demonstrated interdomain flexibility [29]. However, the tightness of the overall domain coupling could not be assessed from the deuterium exchange studies. For the isolated SH3-SH2 fragment of the Src family relative

Table 1. Rotational Diffusion Parameters for SH3 and SH2 of Peptide-Bound FynSH32 (FynSH32*FAK3A*HMTA) at 34°C

Chain[a]	Tensor[b]	$(6D)^{-1}$/ns[c]	$2D_{zz}/(D_{xx} + D_w)$[d]	D_{xx}/D_w[d]	α/Deg[e]	β/Deg[e]	γ/Deg[e]	χ^2/N[f]	$\chi^2/N_{(\alpha=0.10)}$[f]	Q[g]
SH3										
A/B	isotropic	8.47 ± 0.07	—	—	—	—	—	4.15	1.35	
A	oblate	8.00 ± 0.26	0.573 ± 0.043	—	—	131.0 ± 4.3	−115.5 ± 6.5	2.19	1.12	0.0272[h]
B	oblate	8.11 ± 0.20	0.581 ± 0.035	—	—	129.7 ± 3.3	−111.0 ± 6.2	1.31	1.15	7.27×10^{-4}[h]
A	prolate	8.49 ± 0.17	1.359 ± 0.057	—	—	48.7 ± 7.1	−0.3 ± 9.5	3.39	1.15	
B	prolate	8.48 ± 0.16	1.385 ± 0.056	—	—	52.9 ± 6.1	9.0 ± 6.5	3.33	1.12	
A	asymmetric	8.06 ± 0.25	1.486 ± 0.093	0.625 ± 0.053	4.4 ± 6.1	62.0 ± 5.5	−46.3 ± 4.9	1.48	0.99	0.129[i]
B	**asymmetric**	8.15 ± 0.21	1.477 ± 0.077	0.618 ± 0.044	10.1 ± 6.9	59.5 ± 6.2	−45.6 ± 5.0	0.65	0.96	0.0152[i]
SH2										
A/B	isotropic	9.13 ± 0.06	—	—	—	—	—	3.32	1.32	
A	oblate	9.27 ± 0.18	0.745 ± 0.038	—	—	88.6 ± 6.4	−24.3 ± 8.4	3.05	1.12	
B	oblate	9.26 ± 0.18	0.718 ± 0.036	—	—	88.7 ± 5.1	−15.3 ± 5.4	2.21	1.15	
A	**prolate**	9.13 ± 0.19	1.586 ± 0.068	—	—	6.4 ± 4.2	−33.9 ± 38.4	0.64	1.13	1.22×10^{-10}[h]
B	prolate	9.13 ± 0.19	1.564 ± 0.068	—	—	5.6 ± 4.0	−42.8 ± 40.1	0.73	1.13	5.62×10^{-10}[h]
A	asymmetric	8.99 ± 0.25	1.623 ± 0.091	0.869 ± 0.060	−9.8 ± 35.7	7.5 ± 4.7	−52.3 ± 35.4	0.55	1.05	0.208[i]
B	asymmetric	9.04 ± 0.22	1.597 ± 0.081	0.901 ± 0.053	−15.3 ± 37.8	6.9 ± 5.4	−30.4 ± 40.0	0.66	1.02	0.543[i]

[a] Two FynSH32 molecules were found per asymmetric crystal unit, which are referred to as A and B.

[b] Refers to the results obtained assuming different models—an isotropic axially symmetric oblate and prolate and fully asymmetric diffusion tensor. The selected tensor (see main text) is highlighted in bold.

[c,d] Denotes the effective correlation time, $(2D_{xx} + 2D_{yy} + 2D_{zz})^{-1}$, where D_{xx}, D_{yy}, and D_{zz} denote the diagonal elements of the diffusion tensor in its principal frame.

[e] Euler angles α, β, and γ define the rotation that transforms the molecular frame into the principal tensor frame [19]. SH3 and SH2 of A and B, respectively, have here been superimposed to facilitate comparison between A and B.

[f] χ^2/N is the experimental χ^2 per residue. $\chi^2/N_{(\alpha=0.10)}$ denotes the χ^2/N limit for the 90% best Monte Carlo simulations.

[g] The F test-derived Q value denotes the probability that the observed improvement in fit between two diffusion (tensor) models could have occurred by chance [24]. Here, Q values larger than 0.05 are considered to be significant for the rejection of the more complex model.

[h] Compares the isotropic and axially symmetric model.

[i] Compares the axially symmetric and fully asymmetric model. The χ^2/N of the axially symmetric oblate and prolate models can be compared directly, as both models have the same level of complexity.

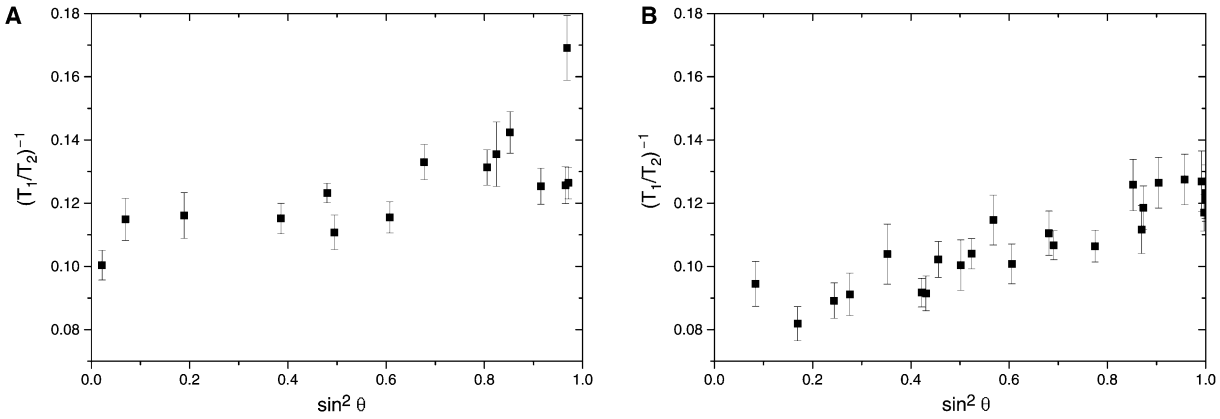

Figure 4. The ^{15}N $(T_1/T_2)^{-1}$ Ratios Used to Determine the Diffusion Tensor of SH3 and SH2 of Peptide-Bound FynSH32 (FynSH32*FAK3A*HMTA)

The ^{15}N $(T_1/T_2)^{-1}$ ratio is sensitive to rotational diffusive motions of the ^{15}N nucleus bearing molecule. Expressed more quantitatively, the (time-averaged) orientation of the H-N vector with respect to the rotational diffusion tensor determines the magnitude of ^{15}N $(T_1/T_2)^{-1}$. The angle θ describes the H-N vector orientation relative to the z axis of the tensor. The wide distribution of data points between $\sin^2\theta$ values of 0–1 shows a good representation of possible H-N orientations and indicates powerful restraints. For isotropic rotational diffusion ("a sphere") all ^{15}N $(T_1/T_2)^{-1}$ ratios would be equal, independent of θ. For SH2 the linear increase in the ^{15}N $(T_1/T_2)^{-1}$ ratio with θ is consistent with molecular reorientation described by a prolate, axially symmetric diffusion tensor. The ^{15}N $(T_1/T_2)^{-1}$ ratios of SH3 exhibit similar features; however, at $\sin^2\theta$ values close to 1, which correspond to H-N vectors close to the x-y plane of the diffusion tensor, the ratios deviate from a straight line, reflecting different lengths of the x and y axes of the diffusion tensor. This is indicative of the fully anisotropic nature of the SH3 diffusion tensor.

Abelson kinase (AblSH32), an NMR study revealed similar isotropic correlation times for AblSH32 (8.85 ± 0.11 ns for SH3 and 9.49 ± 0.07 ns for SH2 [26]) to those of peptide-bound FynSH32 (Table 1). This suggests that there is a similar SH3-SH2 interdomain coupling in AblSH32.

Structural Basis for the SH3-SH2 Coupling of Peptide-Bound FynSH32

Since there are no direct domain contacts between SH3 and SH2 of peptide-bound FynSH32 (Figure 3), interdomain coupling must be mediated by the linker region. In solution, domain coupling will therefore critically depend on the specificity of domain-linker contacts and linker stiffness. The linker contacts SH2 over a surface of ~600 Å^2 and SH3 over ~450 Å^2 (Figure 3), with mainly hydrophobic interactions [10]. The crystal structure of FynSH32 shows the linker region (residues D142–E148) to be well defined (Figure 5A), with B factors only slightly higher than in the protein core but lower than some loop regions (cf. Protein Data Bank entry 1g83). Hydrogen bonds are formed between residues in the linker [8, 10]. Slightly different relative SH3-SH2 domain orientations between the A and B coordinates of the crystal of free FynSH32 [10] suggest that the two conformations found represent "snapshots" from a range of possible domain-domain orientations. We have previously noted low positive ^{15}N-{^1H} NOEs for linker residues, such as I144, in both free and peptide-bound FynSH32 [10] in solution, indicating that the solution state of the linker is less well ordered than in the crystal state. This is consistent with the ability to communicate only relatively small chemical shift changes through the linker region into the adjacent domain (Figures 2 and 3). Thus, it appears that relatively

Table 2. Molecular Alignment Tensors for SH3 and SH2 of Peptide-Bound FynSH32 (FynSH32*FAK3A*HMTA) in 4% (w/v) Bicelle Solution

Chain[a]	A_a/Hz[b]	η[b]	α/Deg[c]	β/Deg[c]	γ/Deg[c]	χ^2/N[d]
SH3						
A	−6.27 ± 0.22	0.26 ± 0.03	14.8 ± 2.5	28.4 ± 1.1	−43.4 ± 4.0	4.18
B	−6.60 ± 0.20	0.21 ± 0.03	12.4 ± 1.9	33.5 ± 1.1	−38.2 ± 4.6	1.88
SH2						
A	−7.85 ± 0.24	0.09 ± 0.03	−81.5 ± 32.2	3.3 ± 1.1	60.8 ± 23.7	2.33
B	−8.15 ± 0.24	0.01 ± 0.02	110.5[e]	176.9	24.1	2.17

[a] Two FynSH32 molecules were found per asymmetric crystal unit, which are referred to as A and B.

[b] η denotes the alignment tensor rhombicity, A_a/A_r, where A_a and A_r denote the axially symmetric rhombic components, respectively, of the traceless alignment tensor in the principal tensor frame.

[c] The Euler angles α, β, and γ define the rotation that transforms the molecular frame into the principal tensor frame [19]. SH2 and SH3 of A and B, respectively, have been superimposed to facilitate comparison between A and B.

[d] χ^2/N is the χ^2 per residue.

[e] No uncertainties are given, as the tensor orientation fluctuates around z and −z and the x and y axes interchange.

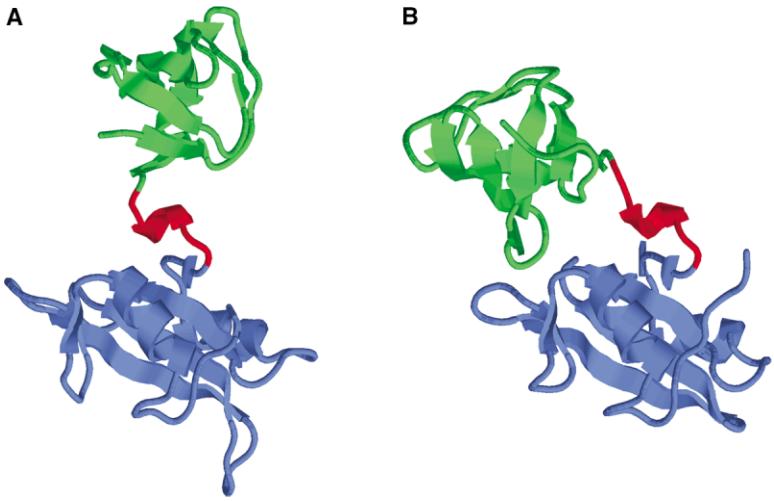

Figure 5. Comparison of the Crystal Structures of FynSH32 and AblSH32

Cartoon representations of the crystal structures of (A) FynSH32 (B form) [10] and (B) AblSH32 [52]. SH2 domains, blue; SH3 domains, green; seven-residue linkers connecting SH3 and SH2, red (Fyn residues 142–148 and Abl residues 139–145). The regular secondary structure elements of both SH2 domains were superimposed (Cα rmsd 0.87 Å), showing distinctly different SH3 domain orientations with respect to the SH2 domain in the crystal structures.

nonspecific, hydrophobic domain-linker contacts, in addition to a somewhat disordered linker in solution, are responsible for the observed domain-domain flexibility within a still considerably coupled environment (intermediately coupled domain state).

Interestingly, the relative SH3-SH2 domain orientation of AblSH32 and FynSH32 are quite different, despite similar linker conformations in the crystal structures (Figure 5). In solution, the AblSH32 linker also exhibits low positive ^{15}N-{^{1}H} NOEs for residues L141 and E142 [30]. In contrast, the B factors of the linker in the crystal structure are slightly higher than in the protein core but lower than in loop regions (cf. Protein Data Bank entry 2abl). The different relative domain orientations of FynSH32 and AblSH32 will be discussed in more detail below.

SH3-SH2 Domain-Domain Orientation of Peptide-Bound FynSH32

The orientations of the diffusion and alignment tensors obtained for SH3 and SH2 of peptide-bound FynSH32 allow the effective average domain-domain orientation [31] to be determined in solution. The relative domain orientation is obtained by rotating the individual domains to align with their principal alignment or diffusion tensor frames (Tables 1 and 2) [32–34]. The average domain orientation of peptide-bound FynSH32 is compared to the crystal structure domain orientation of free FynSH32.

The SH3-SH2 domain-domain inclination (Figure 6) can be defined with relatively high accuracy, but the SH3-SH2 twist (Figure 6) is more difficult to define because of the high axial symmetry of the SH2 domain. The domain twist is therefore left the same as the free FynSH32 crystal structure (B form). Figure 6A shows the SH3-SH2 orientation of peptide-bound FynSH32 after rotating the domains into their common alignment tensor frame as compared to the orientation of the free FynSH32 crystal structure. In both cases the coordinates of the B SH3-SH2 form were used. The observed relative domain orientations deviate by 35.0° ± 9.1°. If the diffusion tensor frames are used rather than alignment tensor frames, the domain-domain inclination is 53.9° ± 10.4° (for B SH3-SH2). The uncertainties of the respective inclination angles include the error from the measurement of experimental data as well as an estimate of the error arising from uncertainties in the backbone FynSH32 crystal structure coordinates, which could be obtained from the comparison of the FynSH32 A and B coordinate sets. Both the alignment and diffusion tensor frames yield very similar directions of inclinations between the domains (see Experimental Procedures). The different extent of the inclination arises from a slightly different orientation of the diffusion and alignment tensor of the SH3 domain. This difference is probably due to the relatively small T_1/T_2 dataset available for the SH3 domain (Figure 4), combined with more-pronounced sensitivity of T_1/T_2 ratios to fast internal H-N motions than to RDCs [32, 34]. Consequently, the alignment tensor result is expected to be more accurate than the diffusion tensor result and is used in the following arguments.

The comparison of the different crystal structures found for free FynSH32 revealed an ~10° variability in SH3-SH2 domain-domain inclination [10]. Thus, considering all uncertainties, the difference in solution state domain orientation of peptide-bound SH3-SH2 compared to free FynSH32 in the crystal (Figure 6A) is significant. Different SH3-SH2 dynamics in the crystal state and crystal-packing restraints provide possible explanations for this difference. The effect of the bound peptides on the domain orientation is expected to be small, since there are only small chemical shift differences between peptide-bound and free FynSH32 states.

Comparison of SH3-SH2 Domain Orientation in Peptide-Bound FynSH32 with the Assembled Inactive Src Kinase

The relative domain orientation of peptide-bound FynSH32 is compared with the SH3-SH2 orientation in the inactive, kinase-bound Src state to gain insight into Src kinase regulation. A crystal structure of the assembled inactive state is available for human Src kinase [1]. Since human Fyn and Src kinases share, besides an overall 74.4% sequence identity, a 100% identity between their SH3-SH2 linkers (Fyn D142-E148 and Src

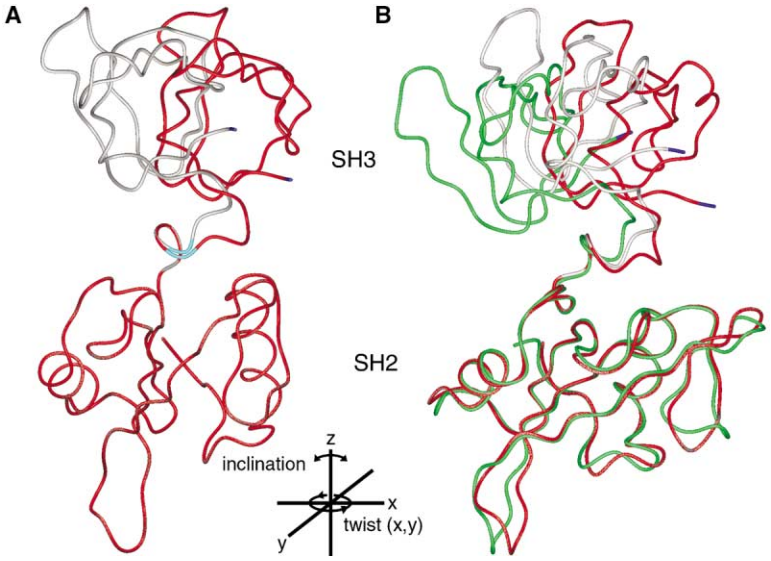

Figure 6. Comparison of the SH3-SH2 Domain-Domain Orientation of Peptide-Bound FynSH32 in Solution with Free FynSH32 in the Crystal State and c-Src SH3-SH2 in the Assembled, Inactive c-Src State

(A) Solution state representation of the domain-domain orientation of peptide-bound FynSH32 (red) in comparison with the crystal structure domain orientation of free FynSH32 (gray; B form). The SH2 domains have been superimposed. The crystal and solution state domain orientations, of SH3 relative to SH2, differ by an inclination of 35.0°. Cα of I144 was chosen as the origin of domain rotations (cyan), as it is known to be flexible in solution (see text). Note that no information about the relative SH3-SH2 domain twist could be obtained and is, therefore, shown in the same orientation as the crystal structure.

(B) Solution state domain orientation of peptide-bound FynSH32 (red) compared to c-Src SH3-SH2 in the assembled, inactive c-Src state (green; Protein Data Bank entry 2src). The SH2 domains have been superimposed on their regular secondary structure elements (Cα rmsd 0.456 Å). It is evident that a large SH3-SH2 domain closure is required to bind to the kinase domain. For comparison the crystal structure of free FynSH32 (B form) is shown in gray.

D141-E147), we expect a comparison between Fyn and Src to be quite meaningful. Figure 6B compares the relative domain orientations of these states. It is evident that a relatively large domain closure is required for the simultaneous binding of SH3 and SH2 to the kinase domain. It is also evident that occupancy of the ligand binding sites does not bring about this closure. In other words, the SH3-SH2 domain pair is bound to the kinase domain in a conformation that deviates distinctly from its average conformation when free in solution. Thus, the relative SH3-SH2 domain orientation in the assembled inactive Src state is dominated by the binding to the kinase domain, whereas the orientation in the active, dissociated state is dominated by the nature of the SH3-SH2 interface. This suggests that the SH3-SH2 domain interface is tuned to facilitate the binding of external ligands rather than the internal kinase domain.

The relative SH3-SH2 orientation in the assembled state appears to be outside the possible range of solution SH3-SH2 orientations of peptide-bound FynSH32 (Figure 6B). The transition from the free FynSH32 state to the assembled kinase-bound state can, thus, be expected to impose strain on the linker in addition to immobilizing relative SH3-SH2 motions. Therefore, the change in SH3-SH2 domain orientation between the free and kinase-bound state is likely to be accompanied by a change in interdomain SH3-SH2 coupling. Such a hypothesis is in agreement with recent molecular dynamics simulations of c-Src and Hck kinases. These simulations suggested a dynamic, Src assembly state-dependent SH3-SH2 coupling that is tight in the assembled inactive state but more flexible when the kinase domain tail (Y527) detaches from the SH2 domain [8].

SH3-SH2 Domain Orientation of FynSH32 Versus AblSH32

Finally, we return to the difference in relative SH3-SH2 domain orientations between the isolated SH3-SH2 fragments of Fyn and Abelson kinase (Figure 5). A comparison of AblSH32 and FynSH32 is worthwhile, since, in contrast to FynSH32, AblSH32 exhibits direct domain-domain contacts in its crystal structure. We thus compared the measured diffusion anisotropies of the SH3-SH2 pairs with the corresponding crystal structures to assess whether AblSH32 and FynSH32 also behave differently in solution.

The diffusion anisotropy of AblSH32 is expected to be significantly lower than that of FynSH32, since the AblSH32 crystal structure is more compact than that of FynSH32 (see Figure 5). The diffusion anisotropies for peptide-bound AblSH32 at 31°C were found to be 1.30 ± 0.09 for SH3 and 1.20 ± 0.08 for SH2 [26] and, thus, significantly lower than for peptide-bound FynSH32 (1.48 ± 0.08 for SH3 and 1.59 ± 0.07 for SH2 at 34°C; Table 1). This is consistent with direct Abl SH3-SH2 domain contacts persisting, at least transiently, in solution [26]. However, it can also not be excluded that this difference arises from a more flexible SH3-SH2 coupling in AblSH32 than in FynSH32. Interestingly, also for a member of the Src kinase family, direct SH3-SH2 domain contacts have been reported. In the crystal structure of the isolated SH3-SH2 fragment of Lck kinase, which has a significantly different SH3-SH2 linker than FynSH32 and SrcSH32 [10], numerous direct SH3-SH2 domain contacts were found [35].

Biological Implications

The Src family of tyrosine kinases is involved in signaling pathways that control the growth and differentiation of cells in response to the activation of cell surface receptors by growth factors, cytokines, or cell surface ligands [36, 37]. Src family kinases possess two ligand binding regulatory domains, SH2 and SH3, which suppress kinase activity when associated with the kinase domain in the cooperatively assembled state and which permit

kinase activity when dissociated from the catalytic domain. The present study has determined the relative SH3-SH2 domain orientation and extent of SH3-SH2 interdomain coupling of the isolated, peptide-bound SH3-SH2 fragment of the Src family kinase Fyn (FynSH32) in solution, by NMR spectroscopy. Isolated SH3-SH2 fragments are expected to correspond to the active, disassembled Src state, where the two domains are uncoupled from the kinase domain. The SH3 and SH2 domains of peptide-bound FynSH32 were found to be significantly coupled yet still exhibit some interdomain flexibility. Substitution of SH3-SH2 linker residues with glycine residues has previously been shown to activate the close Fyn homolog c-Src kinase [8]. The extent of SH3-SH2 coupling thus seems to have been tuned to allow the formation of a stable assembled inactive Src complex yet also flexible enough to allow the SH3 and SH2 domains to bind to alternative, external ligands in the active, disassembled Src state. A large SH3-SH2 domain closure is required for peptide-bound FynSH32 to reach the inactive, kinase-bound SH3-SH2 orientation. Thus, the relative SH3-SH2 domain orientation in the assembled inactive Src state is dominated by the binding to the catalytic domain, whereas the orientation in the active, dissociated state is dominated by the SH3-SH2 interface. Comparison of relative SH3-SH2 domain orientations of Fyn with other isolated SH3-SH2 fragments shows a relatively wide range of possible domain orientations, suggesting that the SH3-SH2 domain orientation has been adapted to their specific external ligands.

Experimental Procedures

Protein Production and NMR Sample Preparation

Protein production and NMR sample preparation of human Fyn kinase SH3-SH2 domains (FynSH32; residues 81–247 with C239S, C240S, and C246S; 19.1 kDa) have been described previously [10]. In brief, T7-*lac* promoter-controlled expression of FynSH32 in *E. coli* BL21(DE3) cells growing at 30°C in M9 minimal medium was induced at an OD_{450} of 0.5 for 6 hr in H_2O or for 12 hr in D_2O solution. FynSH32 was purified from the cell lysate supernatant by phosphotyrosine affinity chromatography. The purification buffer was exchanged by dialysis followed by four ultrafiltration-dilution cycles into 50 mM phosphate buffer (pH 7.0) and 100 mM Na_2SO_4. The protein concentration was determined by UV spectroscopy ($\epsilon_{280} = 28377\ M^{-1}\ cm^{-1}$). Peptides were added in 2-fold excess, and the protein concentration was adjusted to its final value in 50 mM phosphate buffer (pH 7.0), 100 mM Na_2SO_4, and 5% D_2O. Upon addition of peptides the pH was readjusted with NaOH and HCl, if necessary. Small quantities of the chemical shift standard dioxane were added to samples that were used for chemical shift comparisons. A sample with aqueous liquid crystalline phase was prepared by combining buffer and protein at twice the final concentration, with an equal volume of 8% (w/v) 1,2-O-ditridecanyl-*sn*-glycero-3-phosphocholine (DTDPC) and 1,2-O-dihexyl-*sn*-glycero-3-phoshpcholine (DHOPC) in molar ratio of 3:1 [38] in pure water. All samples were contained in NMR microtubes (Shigemi).

Peptide Ligands

The HMTA peptide EPQpYEEIPIYL (1487.6 Da) was purchased from MWG-Biotech AG, Germany. The FAK3A peptide AAAARALPSIPKL (1278.5 Da) and the SM1 peptide ATEPQpYQPGEN (1328.2 Da) were synthesized by the Oxford Centre for Molecular Sciences peptide synthesis facility. All peptides were synthesized with a free C-terminal carboxyl group.

NMR Spectroscopy

NMR experiments were performed on spectrometers operating at ^1H frequencies of 600 and 750 MHz. Backbone resonance assignment of SH32, SH32*SM1, and SH32*FAK32 has been described previously [10]. Assignments of SH32*FAK3A, SH32*HMTA, and SH32*FAK3*HMTA followed directly from comparison of chemical shifts with the previously assigned samples.

As SH2 domains are prone to aggregate [39], we first compared ^{15}N-^1H HSQC spectra [40, 41] of ^{15}N-labeled FynSH32, recorded at 27.5°C and 600 MHz, with acquisition times of 78.8 ms (T_1) and 81.9 ms (T_2), at protein concentrations of 0.2, 0.3, 0.4, 0.6, 0.8, and 1.0 mM. At 1.0 mM some protein precipitated over the course of a few days, and significant changes, indicative of aggregation, were found (data not shown). Consequently, we chose a low protein concentration, 0.3 mM, to compare chemical shifts and to conduct the NMR experiments. To calculate chemical shift differences between the free and peptide-bound FynSH32 states, we recorded ^{15}N-^1H HSQC spectra with acquisition times of 78.8 ms (^{15}N) and 163.8 ms (^1H) for the following samples at 27.5°C and 750 MHz: 0.3 mM ~65% ^2H-, ^{13}C-, and ^{15}N-labeled FynSH32, FynSH32*FAK3A, FynSH32*SM1, FynSH32*HMTA, and FynSH32*FAK3A*HMTA. Prior to zero filling and Fourier transformation, all data sets were apodized using a 25°-shifted squared cosine-bell window function in the ^{15}N dimension and a Lorentzian to Gaussian transformation in the ^1H dimension. The final digital resolution was 3 Hz (0.004 ppm) for ^1H, and 5 Hz (0.07 ppm) for ^{15}N, chemical shifts. Attempts to record carbonyl chemical shifts using the HNCO experiment [42] failed because of low signal to noise ratio. Chemical shifts were referenced with respect to dioxane. All NMR spectra were processed and analyzed with Felix 2.3 (Biosym, San Diego, CA).

^{15}N T_1 and T_2 relaxation times of uniformly ^{15}N-labeled 0.3 mM FynSH32*FAK3A*HMTA were determined at 34°C and 60.8 MHz using pulse sequences described in [43]. Eight relaxation delays ranging from 20 ms to 1.10 s for T_1 and from 8.0 ms to 127.4 ms for T_2, respectively, were used. T_1 and T_2 time constants were extracted as described previously [10]. ^{15}N T_1 and T_2 times of 0.3 mM FynSH32 were recorded previously at 27.5°C [10]. T_2 times were recorded again at 34°C.

Residual dipolar couplings (RDCs) of 0.3 mM ^{15}N-labeled FynSH32*FAK3A*HMTA in anisotropic phase (cf. previous section) were obtained from spectra at 40°C using the in-phase, antiphase scheme [44] with acquisition times of 104.6 ms (^{15}N) and 41.0 ms ($^1H^N$). The buffer used was found to shift the liquid crystalline phase transition to somewhat higher temperatures than pure water. Scalar couplings in isotropic solution were recorded in the absence of liquid crystals at 40°C. Errors were estimated to be 1.0 Hz for SH3 couplings and 1.2 Hz for SH2 couplings.

Rotational Diffusion from ^{15}N Relaxation Data

To test initially for the aggregation state of free FynSH32 and peptide-bound FynSH32 (FynSH32*FAK3A*HMTA), experimental T_1 and T_2 relaxation times were compared with calculated relaxation times as a function of isotropic correlation time and order parameter, S, using the Lipari and Szabo model [45]. For free FynSH32, most residues were found to lie outside the calculated limits (data not shown), suggesting that FynSH32 is still partially aggregated and, consequently, is not accessible to a complete analysis. Peptide-bound FynSH32 was, however, found to lie within calculated limits (data not shown) and, hence, appears to be free of aggregation.

To obtain internuclear H-N vectors, we added hydrogen atoms to the 2.6 Å X-ray crystal structure coordinates of FynSH32 (Protein Data Bank entry 1g83) with the program X-PLOR [46]. T_1/T_2 ratios could reliably be measured for 32 SH3 residues and 45 SH2 residues. ^{15}N-{^1H} NOEs were measured previously for FynSH32 in complex with similar peptides [10] and were used to eliminate residues with ^{15}N-{^1H} NOEs <0.55, i.e., with large-amplitude internal motions. A somewhat low cutoff value is used here because pronounced amide exchange under the solution conditions used lead to generally reduced heteronuclear NOEs. Of the remaining residues, only residues in regular secondary structure were included in the diffusion analysis (17 SH3 and 27 SH2 residues). When using statistical criteria to test for conformational exchange [47], residues I111 and N136 of SH3 and S188 of SH2 stand out with overly large T_1/T_2 ratios. However,

the large T_1/T_2 ratios for N136 and S188 arise only from time-averaged H-N orientations close to parallel to the stable principal z tensor axis, whereas the T_1/T_2 ratio of I111 is extreme, considering its time-averaged H-N vector orientation. Consequently, N136 and S188 were maintained, and I111 was eliminated. One more SH3 and three SH2 residues were eliminated on statistical grounds without significantly affecting the estimation of the diffusion tensor parameters. Nonlinear optimization, of the fit of the experimental T_1/T_2 ratios to calculated values, as a function of alignment tensor parameters, was performed with the program Tensor 2.0 [48] and home-written software [49]. Five hundred Monte Carlo simulations were carried out with Tensor 2.0 to estimate uncertainties in the diffusion tensor parameters and assess the validity of diffusion models. Monte Carlo simulations were performed by generating a new set of input T_1/T_2 ratios, chosen from Gaussian distributions around the back-calculated T_1/T_2 values of the best-fit tensor. Experimental uncertainties were taken as the width of the Gaussian distributions.

A hydrodynamic bead model was used to estimate the diffusion anisotropies of the FynSH32 crystal structure conformations [27, 28]. Beads were placed at the Cα positions, and their radii were adjusted to 2.75 Å to obtain agreement with the experimentally determined isotropic correlation time of peptide-bound FynSH32 (Table 1).

Domain Alignment from Residual Dipolar Couplings

Residual dipolar couplings could be measured for 30 SH3 and for 39 SH2 residues. After eliminating residues with low ^{15}N-{^{1}H} NOE or conformational exchange (cf. previous section), we used 26 couplings for SH3 and 31 for SH2 to determine the molecular alignment tensors for each domain. Three more SH3 and three SH2 residues were eliminated on statistical grounds, without significantly affecting the estimation of the alignment tensor parameters. Nonlinear optimization, of the fit of the experimental residual dipolar couplings to calculated values, as a function of alignment tensor parameters, was performed using the program Module 1.0 [50]. Five hundred Monte Carlo simulations were carried out to estimate uncertainties in the alignment tensor parameters.

Domain-Domain Alignment and Alignment Accuracy

Domain alignments with their principal tensor frames were performed using home-written software. Cα of I144 was chosen as the origin of domain rotations. All tensors reported in Tables 1 and 2 were calculated relative to the molecular frame of the B form of FynSH32, in which the longitudinal molecular axis was taken as the z axis, as depicted in Figure 6. The A structures of SH3 and SH2 were superimposed on the B structures, on their regular secondary structure elements (Cα rmsd SH3 = 0.198 Å and SH2 = 0.230 Å). This permits the direct comparison of the A and B structures and, thus, the estimation of errors resulting from uncertainties in H-N vector orientations in these crystal structures. For B SH3 ($\eta = 0.21$) the alignment tensor x, y, and z axes' inaccuracies are 9.9°, 9.7°, and 2.8°, derived from uncertainties in the measurement of the RDCs, and 2.5°, 6.0°, and 5.8° from the difference between the tensor frames of A and B SH3. Because of the near axial symmetry of the alignment tensor of the SH2 domain ($\eta \leq 0.09$), only the direction of its z axis can be defined with good accuracy. For A SH2, the alignment tensor z axis inaccuracy is 1.9° from RDC uncertainties and 6.1° from the difference between the tensor frames of A and B SH2. The situation for the diffusion tensor principal frames is completely analogous and not explicitly discussed here. An overall inclination ("z axis") inaccuracy of 3.4° is estimated for the alignment tensor, derived from consideration of uncertainties in RDCs alone. An overall inaccuracy of 9.1° results from the inclusion of H-N vector orientation uncertainties (between the A and B crystal structure). Analogously, for the diffusion tensor-derived orientation, an inclination inaccuracy of 10.0° results, considering only uncertainties in T_1/T_2 ratios, and an inclination inaccuracy of 10.4° results when also including H-N orientation uncertainties.

Since the alignment tensor in bicelles is based on asymmetry in molecular shape [47, 51], the principal axes of the diffusion and alignment tensor are expected to agree. For SH2 the agreement is good, with a z interaxis angle of 7.4° ± 6.7° (for B SH2). For SH3 the alignment is similar, with x, y, and z interaxis angles of 12.7° ± 15.5°, 25.5° ± 12.3°, and 26.5 ± 9.0° (for B SH3). These values show that the direction of domain inclination is similar for both the alignment or diffusion tensor-derived domain-domain orientation. The differences for SH3 are mainly responsible for the slightly larger domain inclination obtained for the diffusion tensor result. As discussed in the main text, the relatively small T_1/T_2 dataset available for SH3 (Figure 4) combined with the more pronounced sensitivity of T_1/T_2 ratios than RDCs to internal H-N motions [32, 34] is, most likely, causing this difference.

Acknowledgments

T.S.U. appreciates helpful discussion with Susan Mallet and Jonathan Boyd. We would like to thank Stefan Arold and Martin Noble for making the crystal structures of FynSH32 available prior to publication. We thank Martin Blackledge for making the programs Tensor and Module generally available. T.S.U. acknowledges support from BBSRC. I.D.C. and J.M.W. acknowledge support from the Wellcome Trust and, through the Oxford Centre for Molecular Sciences, from MRC, BBSRC, and EPSRC.

Received: November 7, 2001
Revised: March 26, 2002
Accepted: April 17, 2002

References

1. Xu, W.Q., Harrison, S.C., and Eck, M.J. (1997). Three-dimensional structure of the tyrosine kinase c-Src. Nature *385*, 595–602.
2. Williams, J.C., Weijland, A., Gonfloni, S., Thompson, A., Courtneidge, S.A., Superti-Furga, G., and Wierenga, R.K. (1997). The 2.35 angstrom crystal structure of the inactivated form of chicken Src: a dynamic molecule with multiple regulatory interactions. J. Mol. Biol. *274*, 757–775.
3. Sicheri, F., Moarefi, I., and Kuriyan, J. (1997). Crystal structure of the Src family tyrosine kinase Hck. Nature *385*, 602–609.
4. Sicheri, F., and Kuriyan, J. (1997). Structures of Src-family tyrosine kinases. Curr. Opin. Struct. Biol. *7*, 777–785.
5. Thomas, S.M., and Brugge, J.S. (1997). Cellular functions regulated by Src family kinases. Annu. Rev. Cell Dev. Biol. *13*, 513–609.
6. Supertifurga, G., Fumagalli, S., Koegl, M., Courtneidge, S.A., and Draetta, G. (1993). Csk Inhibition of c-Src activity requires both the Sh2 and Sh3 domains of Src. EMBO J. *12*, 2625–2634.
7. Moarefi, I., LaFevre-Bernt, M., Sicheri, F., Huse, M., Lee, C.H., Kuriyan, J., and Miller, W.T. (1997). Activation of the Src-family tyrosine kinase Hck by SH3 domain displacement. Nature *385*, 650–653.
8. Young, M.A., Gonfloni, S., Superti-Furga, G., Roux, B., and Kuriyan, J. (2001). Dynamic coupling between the SH2 and SH3 domains of c-Src and hck underlies their inactivation by C-terminal tyrosine phosphorylation. Cell *105*, 115–126.
9. Thomas, J.W., Ellis, B., Boerner, R.J., Knight, W.B., White, G.C., 2nd, and Schaller, M.D. (1998). SH2- and SH3-mediated interactions between focal adhesion kinase and Src. J. Biol. Chem. *273*, 577–583.
10. Arold, S.T., Ulmer, T.S., Mulhern, T.D., Werner, J.M., Ladbury, J.E., Campbell, I.D., and Noble, M.E.M. (2001). The role of the Src homology 3-Src homology 2 interface in the regulation of Src kinases. J. Biol. Chem. *276*, 17199–17205.
11. Courtneidge, S.A., Goutebroze, L., Cartwright, A., Heber, A., Scherneck, S., and Feunteun, J. (1991). Identification and characterization of the hamster polyomavirus middle T-antigen. J. Virol. *65*, 3301–3308.
12. Bradshaw, J.M., Grucza, R.A., Ladbury, J.E., and Waksman, G. (1998). Probing the "two-pronged plug two-holed socket" model for the mechanism of binding of the Src SH2 domain to phosphotyrosyl peptides: a thermodynamic study. Biochemistry *37*, 9083–9090.
13. Waksman, G., Shoelson, S.E., Pant, N., Cowburn, D., and Kuriyan, J. (1993). Binding of a high-affinity phosphotyrosyl peptide

to the Src Sh2 domain—crystal-structures of the complexed and peptide-free forms. Cell *72*, 779–790.

14. Ladbury, J.E., Hensmann, M., Panayotou, G., and Campbell, I.D. (1996). Alternative modes of tyrosyl phosphopeptide binding to a Src family SH2 domain: implications for regulation of tyrosine kinase activity. Biochemistry *35*, 11062–11069.
15. Morton, C.J., Pugh, D.J.R., Brown, E.L.J., Kahmann, J.D., Renzoni, D.A.C., and Campbell, I.D. (1996). Solution structure and peptide binding of the SH3 domain from human Fyn. Structure *4*, 705–714.
16. Mulhern, T.D., Shaw, G.L., Morton, C.J., Day, A.J., and Campbell, I.D. (1997). The SH2 domain from the tyrosine kinase Fyn in complex with a phosphotyrosyl peptide reveals insights into domain stability and binding specificity. Structure *5*, 1313–1323.
17. Tessari, M., Gentile, L.N., Taylor, S.J., Shalloway, D.I., Nicholson, L.K., and Vuister, G.W. (1997). Heteronuclear NMR studies of the combined Src homology domains 2 and 3 of pp60 c-Src: effects of phosphopeptide binding. Biochemistry *36*, 14561–14571.
18. Feng, S.B., Chen, J.K., Yu, H.T., Simon, J.A., and Schreiber, S.L. (1994). 2 binding orientations for peptides to the Src Sh3 domain—development of a general-model for Sh3-ligand interactions. Science *266*, 1241–1247.
19. Woessner, D.E. (1962). Nuclear spin relaxation in ellipsoids undergoing rotational Brownian motion. J. Chem. Phys. *37*, 647–654.
20. Bruschweiler, R., Liao, X.B., and Wright, P.E. (1995). Long-range motional restrictions in a multidomain zinc-finger protein from anisotropic tumbling. Science *268*, 886–889.
21. Tjandra, N., and Bax, A. (1997). Direct measurement of distances and angles in biomolecules by NMR in a dilute liquid crystalline medium. Science *278*, 1111–1114.
22. Noble, M.E.M., Musacchio, A., Saraste, M., Courtneidge, S.A., and Wierenga, R.K. (1993). Crystal-structure of the Sh3 domain in human Fyn—comparison of the 3-dimensional structures of Sh3 domains in tyrosine kinases and spectrin. EMBO J. *12*, 2617–2624.
23. Yu, H.T., Chen, J.K., Feng, S.B., Dalgarno, D.C., Brauer, A.W., and Schreiber, S.L. (1994). Structural basis for the binding of proline-rich peptides to Sh3 domains. Cell *76*, 933–945.
24. Press. W.H., Flannery, B.P., Teukosky, S.A., and Vetterling, W.T. (1990). Numerical Recipes in C (New York: Cambridge University Press).
25. Saupe, A., and Englert, G. (1963). High-resolution nuclear magnetic resonance spectra of orientated molecules. Phys. Rev. Lett. *11*, 462–464.
26. Fushman, D., Xu, R., and Cowburn, D. (1999). Direct determination of changes of interdomain orientation on ligation: use of the orientational dependence of N-15 NMR relaxation in Abl SH(32). Biochemistry *38*, 10225–10230.
27. Delatorre, J.G., Navarro, S., Martinez, M.C.L., Diaz, F.G., and Cascales, J.J.L. (1994). Hydro—a computer-program for the prediction of hydrodynamic properties of macromolecules. Biophys. J. *67*, 530–531.
28. Delatorre, J.G., and Bloomfield, V.A. (1981). Hydrodynamic properties of complex, rigid, biological macromolecules—theory and applications. Q. Rev. Biophys. *14*, 81–139.
29. Engen, J.R., Smithgall, T.E., Gmeiner, W.H., and Smith, D.L. (1999). Comparison of SH3 and SH2 domain dynamics when expressed alone or in an SH(3+2) construct: the role of protein dynamics in functional regulation. J. Mol. Biol. *287*, 645–656.
30. Gosser, Y.Q., Zheng, J., Overduin, M., Mayer, B.J., and Cowburn, D. (1995). The solution structure of Abl Sh3, and its relationship to Sh2 in the Sh(32) construct. Structure *3*, 1075–1086.
31. Skrynnikov, N.R., Goto, N.K., Yang, D.W., Choy, W.Y., Tolman, J.R., Mueller, G.A., and Kay, L.E. (2000). Orienting domains in proteins using dipolar couplings measured by liquid-state NMR: differences in solution and crystal forms of maltodextrin binding protein loaded with beta-cyclodextrin. J. Mol. Biol. *295*, 1265–1273.
32. Tjandra, N., Omichinski, J.G., Gronenborn, A.M., Clore, G.M., and Bax, A. (1997). Use of dipolar H-1-N-15 and H-1-C-13 couplings in the structure determination of magnetically oriented macromolecules in solution. Nat. Struct. Biol. *4*, 732–738.
33. Losonczi, J.A., Andrec, M., Fischer, M.W.F., and Prestegard, J.H. (1999). Order matrix analysis of residual dipolar couplings using singular value decomposition. J. Magn. Reson. *138*, 334–342.
34. Tjandra, N., Garrett, D.S., Gronenborn, A.M., Bax, A., and Clore, G.M. (1997). Defining long range order in NMR structure determination from the dependence of heteronuclear relaxation times on rotational diffusion anisotropy. Nat. Struct. Biol. *4*, 443–449.
35. Eck, M.J., Atwell, S.K., Shoelson, S.E., and Harrison, S.C. (1994). Structure of the regulatory domains of the Src-family tyrosine kinase Lck. Nature *368*, 764–769.
36. Bolen, J.B. (1993). Nonreceptor tyrosine protein-kinases. Oncogene *8*, 2025–2031.
37. Brown, M.T., and Cooper, J.A. (1996). Regulation, substrates and functions of src. Biochim. Biophys. Acta *1287*, 121–149.
38. Ottiger, M., and Bax, A. (1999). Bicelle-based liquid crystals for NMR-measurement of dipolar couplings at acidic and basic pH values. J. Biomol. NMR *13*, 187–191.
39. Farrow, N.A., Muhandiram, R., Singer, A.U., Pascal, S.M., Kay, C.M., Gish, G., Shoelson, S.E., Pawson, T., Formankay, J.D., and Kay, L.E. (1994). Backbone dynamics of a free and a phosphopeptide-complexed Src homology 2 domain studied by N-15 NMR relaxation. Biochemistry *33*, 5984–6003.
40. Boyd, J., Soffe, N., John, B., Plant, D., and Hurd, R. (1992). The generation of phase-sensitive 2d N-15-H-1 spectra using gradient pulses for coherence-transfer-pathway selection. J. Magn. Reson. *98*, 660–664.
41. Grzesiek, S., and Bax, A. (1993). The importance of not saturating H2O in protein NMR—application to sensitivity enhancement and NOE measurements. J. Am. Chem. Soc. *115*, 12593–12594.
42. Salzmann, M., Pervushin, K., Wider, G., Senn, H., and Wuthrich, K. (1998). TROSY in triple-resonance experiments: new perspectives for sequential NMR assignment of large proteins. Proc. Natl. Acad. Sci. USA *95*, 13585–13590.
43. Farrow, N.A., Zhang, O.W., Formankay, J.D., and Kay, L.E. (1994). A heteronuclear correlation experiment for simultaneous determination of N-15 longitudinal decay and chemical-exchange rates of systems in slow equilibrium. J. Biomol. NMR *4*, 727–734.
44. Ottiger, M., Delaglio, F., and Bax, A. (1998). Measurement of J and dipolar couplings from simplified two-dimensional NMR spectra. J. Magn. Reson. *131*, 373–378.
45. Lipari, G., and Szabo, A. (1982). Model-free approach to the interpretation of nuclear magnetic-resonance relaxation in macromolecules. 1. Theory and range of validity. J. Am. Chem. Soc. *104*, 4546–4559.
46. Brünger, A.T. (1992). X-PLOR Version 3.1: A System for X-ray Crystallography and NMR (New Haven, CT: Yale University Press).
47. de Alba, E., Baber, J.L., and Tjandra, N. (1999). The use of residual dipolar coupling in concert with backbone relaxation rates to identify conformational exchange by NMR. J. Am. Chem. Soc. *121*, 4282–4283.
48. Dosset, P., Hus, J.C., Blackledge, M., and Marion, D. (2000). Efficient analysis of macromolecular rotational diffusion from heteronuclear relaxation data. J. Biomol. NMR *16*, 23–28.
49. Werner, J.M., Campbell, I.D., and Downing, A.K. (2001). Shape and dynamics of a calcium binding EGF domain pair investigated by 15N-NMR relaxation. Methods Mol. Biol. *173*, 285–300.
50. Dosset, P., Hus, J.C., Marion, D., and Blackledge, M. (2001). A novel interactive tool for rigid-body modeling of multi-domain macromolecules using residual dipolar couplings. J. Biomol. NMR *20*, 223–231.
51. Zweckstetter, M., and Bax, A. (2000). Prediction of sterically induced alignment in a dilute liquid crystalline phase: aid to protein structure determination by NMR. J. Am. Chem. Soc. *122*, 3791–3792.
52. Nam, H.J., Haser, W.G., Roberts, T.M., and Frederick, C.A. (1996). Intramolecular interactions of the regulatory domains of the Bcr-Abl kinase reveal a novel control mechanism. Structure *4*, 1105–1114.